ACS APPLIED MATERIALS & INTERFACES

Research Article

www.acsami.org

Open Access on 01/16/2015

Nanofiber Scaffolds with Gradients in Mineral Content for Spatial Control of Osteogenesis

Wenying Liu,[†] Justin Lipner,[‡] Jingwei Xie,[‡,§] Cionne N. Manning,[⊥] Stavros Thomopoulos,*[,⊥] and Younan Xia*[,¶,†]

[†]School of Chemical and Biomolecular Engineering, Georgia Institute of Technology, Atlanta, Georgia 30332, United States

[‡]Department of Biomedical Engineering, Washington University, St. Louis, Missouri 63130, United States

[⊥]Department of Orthopaedic Surgery, Washington University, St. Louis, Missouri 63110, United States

[¶]The Wallace H. Coulter Department of Biomedical Engineering, School of Chemistry and Biochemistry, Georgia Institute of Technology, Atlanta, Georgia 30332, United States

Supporting Information

ABSTRACT: Reattachment of tendon to bone has been a challenge in orthopedic surgery. The disparate mechanical properties of the two tissues make it difficult to achieve direct surgical repair of the tendon-to-bone insertion. Healing after surgical repair typically does not regenerate the natural attachment, a complex tissue that connects tendon and bone across a gradient in both mineral content and cell phenotypes. To facilitate the regeneration of the attachment, our groups have developed a nanofiber-based scaffold with a graded mineral coating to mimic the mineral composition of the native tendon-to-bone insertion. In the present work, we evaluated the ability of this scaffold to induce graded osteogenesis of adipose-derived mesenchymal stem cells (ASCs). Results from 3-(4,5-dimethylthiazol-2-yl)-2,5-diphenyltetrazolium bromide assay and proliferating cell nuclear antigen staining indicated that cell proliferation was negatively correlated with the mineral content. In contrast, alkaline phosphatase staining, an indicator of osteogenesis, was positively correlated with the mineral content. Likewise, runt-related transcription factor 2 (an early marker of osteoblast differentiation) and osteocalcin (a late marker of osteoblast differentiation) immunostaining were both positively correlated with the mineral content. These results indicate that a gradient in mineral content on the surface of a nanofiber scaffold is capable of inducing graded differentiation of ASCs into osteoblasts for enthesis repair.

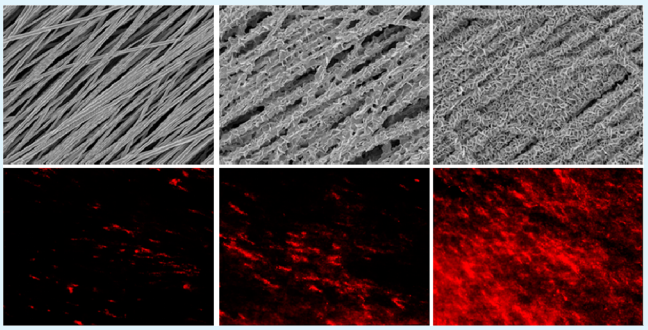

KEYWORDS: *electrospun nanofiber, mineral gradient, adipose-derived mesenchymal stem cell (ASC), osteogenesis, tendon-to-bone insertion, tissue engineering*

INTRODUCTION

The functional integration of tendon with bone after injury is a well-known clinical challenge. For example, the reported failure rates for rotator cuff repair, which typically requires tendon-to-bone healing, range from 20% (for the repair of small tears) to 94% (for the repair of massive tears).[1,2] The high failure rate is likely due to a lack of regeneration of the natural tendon-to-bone attachment (enthesis).[3] The uninjured enthesis consists of a functionally graded transitional tissue, with spatial variations in its extracellular matrix (ECM) composition, structural organization, cell phenotype, and mechanical properties.[3,4] For example, the attachment shows a transition from compliant tendon, which contains no mineral, to stiff bone, which contains ∼50 vol % mineral, across a spatial gradient in mineral content.[5,6] The mineral stiffens the ECM, resulting in a more than a 100-fold increase in modulus for the enthesis near the bone as compared to that near the tendon.[7] In addition to compositional differences, the phenotypes of the cells residing in tendon, bone, and enthesis are distinct as well. While tendon is populated by fibroblasts, the bone tissue is populated by osteoblasts, osteocytes, and osteoclasts.[8] A strong mechanical attachment between tendon and bone is established *via* a strucutral gradient in ECM, which is synthesized and maintained by gradients in cell types.[9] Unfortunately, surgical repair of the injured insertion does not recreate these gradients,[2] leading to high clinical failure rates. In order to improve tendon-to-bone repair, more advanced therapies are needed to promote regeneration of the complex natural enthesis.

Tissue engineering has emerged as a promising strategy for enhancing tendon-to-bone repair. This approach is aimed primarily at developing a cell-seeded scaffold that can

Received: November 27, 2013
Accepted: January 16, 2014
Published: January 16, 2014

reproduce the native, graded structure of the enthesis.[10−13] Such a scaffold may facilitate surgical repair by promoting regeneration, leading to the functional recovery of a robust attachment. A number of important criteria should be incorporated into the design, including: (i) spatially graded mineral content and (ii) cell phenotypes that gradually change from tendon fibroblast to bone osteoblast along the scaffold.[14] Scaffolds based on electrospun nanofibers are attractive for orthopedic tissue engineering due to their biomimetic potential and physiological similarity to the ECM.[15−19] Previously, our groups demonstrated the fabrication of nanofiber-based scaffolds with spatial gradients in mineral content to mimick the composition and mechanics of the enthesis.[20] In this work, we systematically investigated the cellular responses to this novel type of scaffold *in vitro* using a clinically relevant cell source. An appropriate cell source for tendon-to-bone repair should be capable of both tenogenesis and osteogenesis. Adipose-derived mesenchymal stem cells (ASCs) are promising candidates due to their ability to differentiate into both cell phenotypes. ASCs have a number of advantages over other mesenchymal stem cell (MSC) sources: (i) they can be harvested using minimally invasive procedures; (ii) they are available in abundant quantities; (iii) they possess the ability to differentiate into multiple mesenchymal lineages, and (iv) they display immunosuppressive capabilities.[21−25] Therefore, the use of autologous ASCs for enthesis repair represents a promising new direction.

The goal of the current study was to investigate the ability of a nanofiber-based scaffold, with a spatial gradient in mineral content, to induce spatially controlled osteogenesis of ASCs. The gradient in mineral content corresponds to a gradient in local scaffold modulus.[20] Since stem cells respond to both the stiffness and composition of the substrate, we hypothesized that ASC osteogenesis would be positively correlated with the mineral content whereas the proliferation of the ASCs would be negatively correlated with the mineral content.

MATERIALS AND METHODS

Materials. Poly(lactic-*co*-glycolic) acid (PLGA) ($M_w \approx 50\,000-75\,000$, lactide/glycolide = 85:15), dichloromethane (DCM), dimethylformaldehyde (DMF), acetic acid, and all chemicals used for preparation of 10× concentrated simulated body fluid (10SBF) were obtained from Sigma-Aldrich (St. Louis, MO). All chemicals were used as received.

Electrospinning and Plasma Treatment. The solution for electrospinning was prepared by dissolving PLGA in a mixture of DCM and DMF (with a volume ratio of 80:20) at a total concentration of 25%. The solution was loaded into a 5 mL plastic syringe with a 23 1/2-gauge needle attached and dispensed using a syringe pump. The injection rate was 0.5 mL/h. The fibers were collected using a rotating mandrel at a speed of 2 m/s. The distance between the tip of needle and the collector was about 20 cm, and a voltage of 15 kV was applied. The electrospun nanofiber scaffold was then transferred to a metal frame for plasma treatment. Plasma treatment was conducted in a plasma cleaner (PE50, Unitronics, NV) for 3 min to make the scaffold hydrophilic and completely wettable by the mineral coating solution.

Generation of a Mineral Gradient. We prepared 10SBF as described previously.[26] A stock solution containing NaCl, KCl, $CaCl_2$, $MgCl_2$, and $NaH_2PO_4{\cdot}H_2O$ was prepared in advance, and $NaHCO_3$ was added at room temperature prior to initiating the mineralization process. To create a gradient in mineral along the scaffold length, the as-prepared mineral solution was loaded into a 50 mL plastic syringe and fed continuously into a glass vial using a syringe pump at a feeding rate of 36 mL/h.[20] A uniaxially aligned nonwoven mat of electrospun nanofibers supported on a metal frame was placed inside the vial at a tilting angle of 45 degrees relative to the horizontal direction. Presoaking the scaffold in 10SBF for 0.5 h prior to the coating process allowed for the creation of mineral gradient with a higher slope of increasing mineral content.

Characterization of Mineral Content and Morphology. A scanning electron microscope (SEM; Ultra 60, Carl Zeiss, Thornwood, NY) was used to examine the morphologies of deposited mineral crystals at different locations along the long axis of the nanofiber scaffolds. The atomic ratio Ca/(C+Ca) was determined at different locations along the length of the scaffold using energy dispersive X-ray (EDX). Three samples were examined.

ASC Isolation, Culture, and Seeding. All animal protocols were approved by the Washington University Animal Studies Committee. Adipose-derived stem cells were isolated from young Sprague−Dawley rats obtained from Charles River Laboratories (Wilmington, MA) using standard techniques.[27] Animals were sacrificed using carbon dioxide narcosis. Fat was isolated from the subdermal abdomen and minced using scalpel blades. The minced fat was then placed into >5 times its volume of 0.2 wt % Collagenase A (Roche, Indianapolis, IN) solution for 2 h in a cell culture incubator (37 °C, 95% relative humidity, 5% CO_2). After incubation, the solution was centrifuged and the fat and collagenase solution were removed. The remaining suspension was filtered using a Nylon 100 μm filter (Fisher Scientific, Pittsburgh, PA) and cultured in a standard proliferation medium: α-Minimum Essential Medium (MEM, Invitrogen, Carlsbad, CA), 10% fetal bovine serum (FBS, Invitrogen), 1:1000 penicillin/streptomycin (Invitrogen), and 1% Amphotericin B (Fisher Scientific). The culture was washed after 24 h with phosphate buffered saline (PBS, Invitrogen) to remove any remaining debris and passaged once to ensure adherence selection. The cells were incubated at 37 °C under 95% relative humidity and 5% CO_2. The medium was changed every 2 days until 80% confluence. Cells were seeded onto rectangular nanofiber scaffolds (1 × 5 cm^2) glued to Petri dishes; 2 × 10^5 cells (as determined by hemocytometer counting) were seeded onto each scaffold. Samples were divided into two groups, and the first group was cultured in proliferation medium (described above) while the second group was cultured in osteogenic medium: α-MEM, 10% FBS, 1:1000 penicillin/streptomycin, 2.16 g/L β-glycerophosphate (Sigma-Aldrich), and 50 mg/L ascorbic acid (Sigma-Aldrich). All ASCs were isolated from one rat. All cells for this study were used at passage 2. The cells isolated in the present work demonstrated pluipotency based on standard adipogenic, osteogenic, chonodrogenic, and tenogenic protocols reported in our previous study.[28]

Live/Dead Assay. A live/dead assay kit (Invitrogen), consisting of calcein AM and ethidium homodimer-1 (EthD-1), was used to assess cell viability and cell distribution. The intracellular esterase present in live cells converts calcein AM, a cell permeable dye, to calcein, resulting in a bright green fluorescence. EthD-1 can only penetrate damaged membranes of dead cells where it binds to nucleic acids, producing intense red fluorescence. Briefly, the cells were incubated for 30 min with regular culture medium supplemented with 2 μM calcein AM and 4 μM EthD-1 and analyzed via fluorescent microscopy (Leica DMI6000, Buffalo Grove, IL). Three samples from each group were analyzed at each time point.

Cell Viability Assay. The relative number of cells on each scaffold was quantitatively measured by the 3-(4,5-dimethylthiazol-2-yl)-2,5-diphenyltetrazolium bromide (MTT) assay (Invitrogen). MTT is a tetrazole that is metabolized and reduced to purple formazan in live cells. Each 1 × 5 cm^2 scaffold was cut into 10 pieces, resulting in 0.5 × 1 cm^2 area per piece. For each time point, 3 samples were analyzed for each type of culture medium. Assays were carried out in 12-well plates, and 40 μL of MTT solution in PBS (5 mg/mL) was added to each well and incubated at 37 °C for 4 h. Culture medium was then withdrawn, and 1 mL of isopropanol was added to each well to completely dissolve formazan crystals throughout the scaffolds. Absorbance was measured at 560 nm using a spectrophotometer (Infinite 200 Pro, TECAN, Morrisville, NC). All final data were normalized to the dry weight of each scaffold.

ALP Staining. Alkaline phosphatase (ALP) staining was performed using Vector Red Alkaline Phosphatase Substrate Kit (SK-5100, Vector Laboratories, Burlingame, CA) according to the manufacturer's instructions. ALP activities were quantified on the basis of the mean pixel intensity using Image J. Three samples from each group were analyzed at each time point.

Immunocytochemistry. Proliferating cell nuclear antigen (PCNA) was purchased from Invitrogen. Antibodies for runt-related transcription factor 2 (Runx2) and osteocalcin (OCN) were purchased from Abcam (Cambridge, MA). The scaffolds were fixed in 3.7% formaldehyde (Sigma-Aldrich) in PBS. The cells were then permeabilized in 0.1% Triton X-100 (Sigma-Aldrich) in PBS for 1 h. Subsequently, the cells were blocked with 5% normal goat serum (Sigma-Aldrich) and 1.5% bovine serum albumin (Sigma-Aldrich) in PBS for 1 h. Each of the primary antibodies (dilution: PCNA 1:20, Runx2 1:100, and OCN 1:200) was then applied separately to scaffold samples in blocking buffer at 4 °C overnight. After washing, the samples were incubated with Alexa Fluor 488 goat antimouse IgG (1:200 in PBS, Invitrogen) for 1 h, washed, and observed under the fluorescence microscope. Three samples from each group were analyzed at each time point.

Statistical Analysis. Results are presented in the form of mean ± standard deviation, with "*N*" indicating the number of samples per group. A three factor analysis of variance (ANOVA) was used to determine the effects of culture time, culture medium, and mineral content on cell distribution and ALP activities on the scaffolds. Tukey's posthoc test was used for all pairwise comparisons, and significance was attained at $p < 0.05$. Statistical analyses were performed with Systat 13 (Crane Software International, Chicago, IL).

RESULTS AND DISCUSSION

Fabrication of Nanofiber Scaffolds with Spatial Gradients in Mineral Content. The average diameter of the nanofibers was ~200 nm. According to the literature, the overall porosity of the scaffold was ~85%.[29] Figure 1 shows a photograph of our approach for generating a graded coating of calcium phosphate on a nonwoven mat of electrospun nanofibers. Since the amount of mineral deposited on the nanofibers from the mineralization solution is directly proportional to the immersion time, we were able to generate a mineral gradient along the long axis of the scaffold by varying the immersion time. In the present study, this was achieved by adding the mineralization solution at a constant rate into a beaker containing the scaffold (supported on a substrate) in a tilted orientation. The gradient profile was determined by the concentration of the mineralization solution, the titling angle of the substrate, and the solution feeding rate. To improve the hydrophilicity of the nanofibers and activate their surfaces for calcium phosphate deposition, the scaffolds were exposed to air plasma treatment. For the mineralization solution, we used 10SBF, in which the concentrations of calcium and phosphate ions were ten times of those found in human plasma. Rapid deposition of minerals (within a period of 2−6 h) was induced by mixing the 10SBF with $NaHCO_3$.[26] Our previous study revealed that fiber incubation in 10SBF for 2 h could generate a relatively thick layer of calcium phosphate on a mat of gelatin-coated electrospun poly (ε-caprolactone) (PCL) nanofibers.[30] A similar phenomenon was also observed by Yang and co-workers for plasma-treated, electrospun PCL nanofibers after immersion in 10SBF for 2 h.[31]

The variation in immersion time resulted in the formation of a continuous gradient in mineral content along the substrate. Figure 2 shows SEM images of uniaxially aligned PLGA nanofibers covered with a graded mineral coating. The longitidinal position along the scaffold was registered to the interface set by air and the 10SBF solution, which corresponded to $d = 0$. Figure 2 shows images of the scaffold taken at positions of $d = 1$, 2, 3, and 5 cm. The density and the thickness of the mineral coating increased gradually from 1 to 5 cm. The relative amount of mineral was determined by EDX measure-

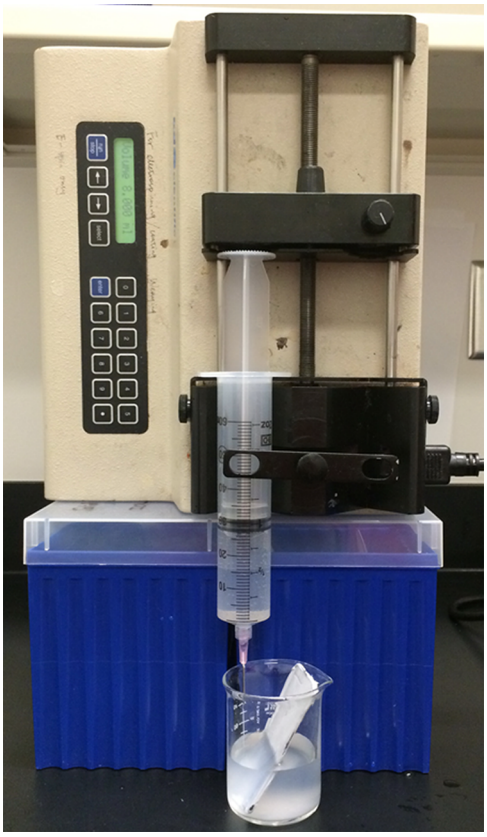

Figure 1. Photograph of the setup used for fabricating a nanofiber scaffold with a gradient in mineral content. As the 10SBF was added into the beaker, the minerals were gradually deposited on the nanofiber scaffold that was immersed in the solution. As the level of the solution rose, a gradient in mineral content formed due to the difference in immersion time between the top and bottom ends of the scaffold.

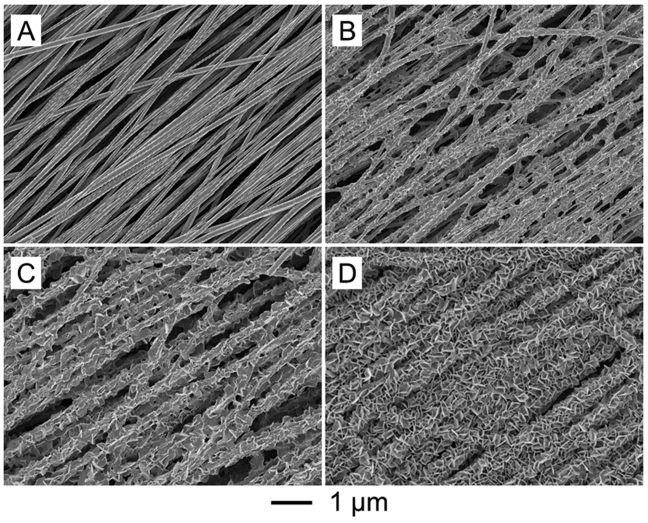

Figure 2. SEM images of calcium phosphate coatings on a plasma-treated nonwoven mat of PLGA nanofibers at (A) 1, (B) 2, (C) 3, and (D) 5 cm from one end of the scaffold.

ments. As shown in Figure 3, the atomic Ca/(Ca+C) ratio changed from ~2% to ~50% over the distance of 5 cm along

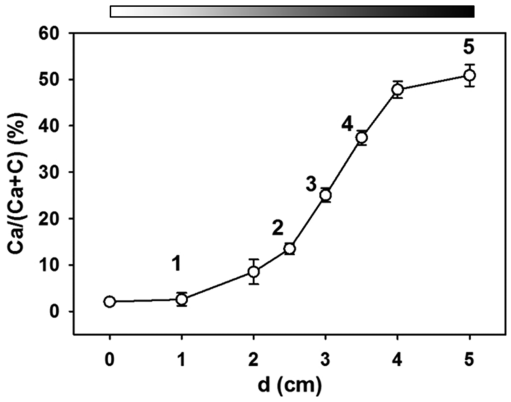

Figure 3. EDX quantification of the gradient in mineral coating (N = 3). The mineral content increased monotonically along the 5 cm length of the scaffold. The grayscale legend above the plot shows the gradient in mineral coating, with the highest mineral level shown in black.

the scaffold. As indicated in Figure 3, five locations along the long axis of each scaffold were analyzed for the experiments described below. Locations 1 and 5 were chosen to represent the unmineralized and fully mineralized regions, respectively, whereas locations 2–4 were chosen to be equidistant from each other in the central portion of the scaffold.

Cell Viability. In order to investigate the response of the ASCs to the mineral gradients on the scaffolds, cells were cultured on the scaffolds in the presence of either proliferation medium or osteogenic medium for 2 h, 7 days, 14 days, and 28 days. All the data pertaining to cells cultured in osteogenic medium can be found in the Supporting Information. Cell viability was visualized by live/dead staining at the end of each time period. The first columns in Figures S1 and S2, Supporting Information, show that ASCs were distributed homogeneously on the scaffolds and remained highly viable 2 h post initial seeding. The ASCs successfully adhered to the scaffolds, and cell density increased with prolonged duration of incubation time in both types of culture medium (Figures S1 and S2, Supporting Information). Under both conditions, the ASCs maintained high viability at all locations on the scaffolds regardless of mineral content.

To visualize proliferative activity in the ASCs, we performed PCNA staining for cells after 7 and 14 days of culture (Figure 4). In both culture media, PCNA staining was negatively correlated with mineral content. For the proliferative group at day 7, ~95% of the ASCs at location 1 (no mineral) maintained their proliferative status, whereas only ~50% of the cells at location 5 (high mineral) were proliferative (Figure 4A–C). At day 14, although the cell density remained relatively unchanged, almost all of the ASCs at location 5 were negative for PCNA staining (Figure 4D–E). A similar, opposing gradient (with regard to that of the mineral gradation) of the PCNA staining was also observed for ASCs in the osteogenic group (Figure S3, Supporting Information).

We further conducted MTT assay to analyze the response of ASCs to the scaffold. During the initial seeding process, ASCs were distributed homogeneously on the scaffolds, with similar cell densities on all samples. Figure 5A shows the absorbance of formazan crystals (dissolved in iso-propanol) metabolized from MTT by live ASCs in the proliferation group. The set of columns for day 1 had similar values of absorbance, indicating comparable cell densities across the entire length of each scaffold. However, a gradient in cell density, negatively correlated with the mineral content, began to appear at day 7 and became more prominent with increasing culture time. Specifically, the cell density was the lowest at location 5 (corresponding to the location with the highest mineral content) and the highest at location 1 (corresponding to the location with no mineral) for each scaffold. A gradient in cell density, negatively correlated with mineral content, was found

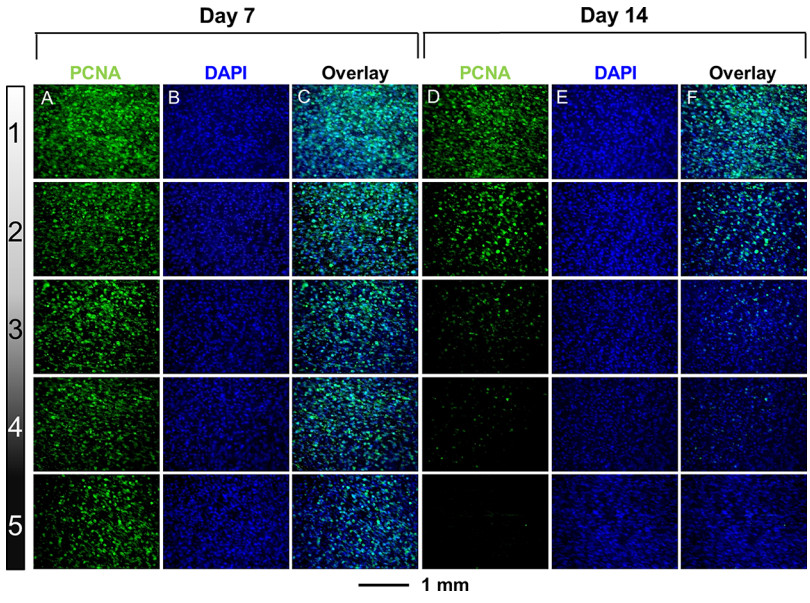

Figure 4. PCNA staining of ASCs seeded on aligned nanofibers with a spatial mineral gradient after culture for (columns A–C) 7 days and (columns D–F) 14 days in proliferation medium. (A, D) PCNA staining of ASCs on day 7 and 14, respectively. (B, E) DAPI staining of ASCs on day 7 and 14, respectively. (C) Superimposed images of (A) and (B). (F) Superimposed images of (D) and (E). Cellular density (as visualized with DAPI) was similar along the length of the scaffold and over time. PCNA staining was negatively correlated with mineral content.

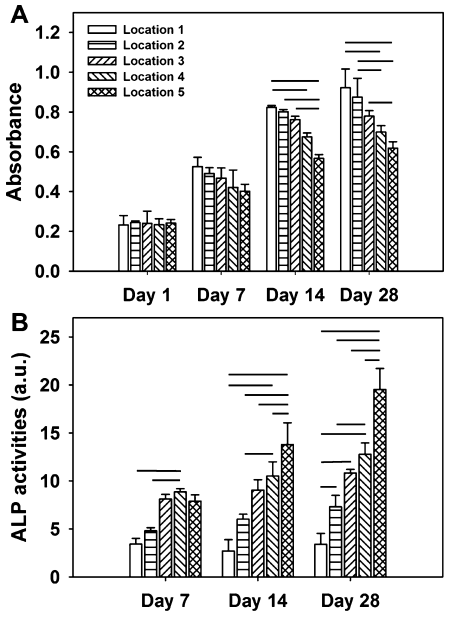

Figure 5. (A) Quantification of cell proliferation on aligned nanofibers with a graded mineral coating for 1, 7, 14, and 28 days. The data were obtained using the MTT assay. Proliferation was negatively correlated with mineral content in proliferation medium. (B) Quantification of ALP activity of ASCs seeded on aligned nanofibers with a graded mineral coating for 7, 14, and 28 days. There was an increase in ALP expression by ASCs over time, and this expression was positively correlated with mineral content. Significance indicated by lines over the bars.

in the osteogenic group as well, but with a remarkably lower absorbance at all of the time points compared to the proliferation group (Figure S4, Supporting Information). All three factors (culture medium, culture time, and location) contributed significantly to these differences in absorbance ($p < 0.05$).

Osteogenesis. To understand the influence of mineral gradient on ASC differentiation, osteogenesis was evaluated for cells in both proliferation and differentiation medium at 7, 14, and 28 days post seeding. ALP is an enzyme that is highly expressed in bone cells, which interacts with organic phosphates present in tissue fluids, leading to the accumulation of inorganic phosphate necessary for mineralization. This phosphate binds to locally present calcium ions to generate calcium phosphate crystals and stimulate bone formation.[32] Therefore, ALP is commonly used as an early marker of osteogenesis.[33,34]

Images of the localized staining of ALP, for the proliferation and osteogenic groups, can be found in Figures S5 and S6, Supporting Information, respectively. There was an increase in ALP expression by ASCs over time, which was positively correlated with mineral content. Quantification of ALP activity was performed by assessing the mean pixel intensity of images using the software Image J. The intensities of ALP activities at different locations are shown in Figure 5B. There were significant effects ($p < 0.05$) on ALP activity for the factors location (i.e., mineral content), culture time, and culture medium at all of the time points except for day 1. This analysis supported the staining results: (i) there was a positive correlation between ALP activity and spatial location (i.e., mineral content), and (ii) ALP activity increased with culture time. Statistically, regardless of culture medium or culture time, there was a significant effect of location (mineral content) on ALP activity ($p < 0.05$).

To further evaluate osteogenesis on the graded scaffolds, immunocytochemistry was performed for Runx2 (an early marker of osteoblast differentiation) and OCN (a late marker of osteoblast differentiation). Runx2 is an essential early transcription factor that drives MSCs toward osteoblast differentiation.[35−38] For instance, Runx2-deficient mice lack

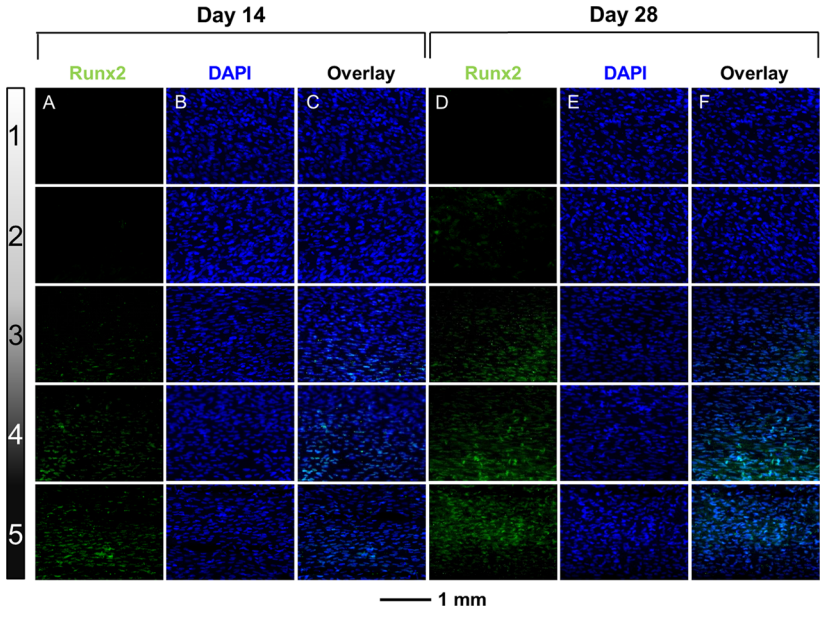

Figure 6. Runx2 staining of ASCs seeded on aligned nanofibers with a spatial mineral gradient after culture for (A−C) 14 and (D−F) 28 days in proliferation medium. (A, D) Runx2 staining of ASCs on day 14 and 28, respectively. (B, E) DAPI staining of ASCs on day 14 and 28, respectively. (C) Superimposed images of (A) and (B). (F) Superimposed images of (D) and (E). Runx2 staining was positively correlated with increasing mineral content and increased with culture time.

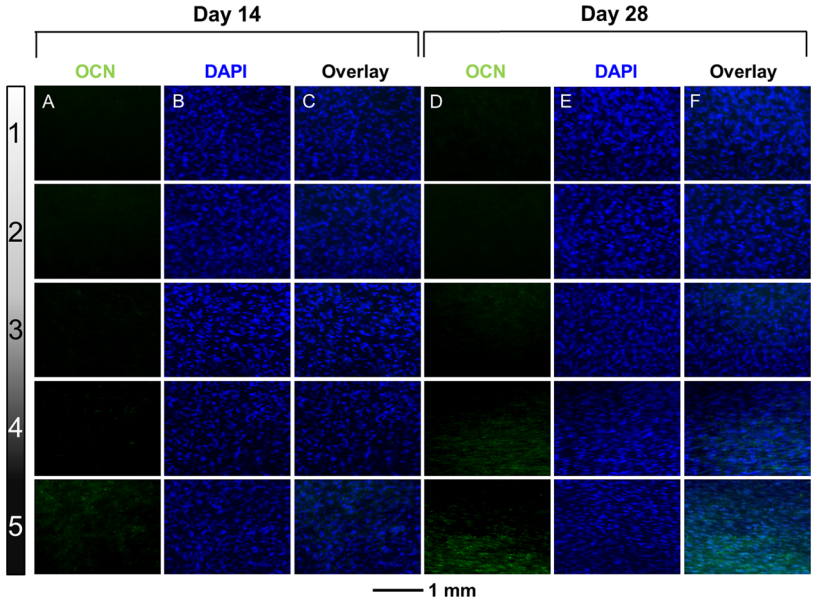

Figure 7. OCN staining of ASCs seeded on aligned nanofibers with a spatial mineral gradient after culture for (A−C) 14 and (D−F) 28 days in proliferation medium. (A, D) OCN staining of ASCs on day 14 and 28, respectively. (B, E) DAPI staining of ASCs on day 14 and 28, respectively. (C) Superimposed images of (A) and (B). (F) Superimposed images of (D) and (E). OCN staining was positively correlated with increasing mineral content and increased with culture time.

bone formation due to the absence of osteoblasts.[39] We were able to detect Runx2 expression as early as day 7 in the osteogenic group whereas no positive staining could be observed for the proliferation group at this time point. Results from Runx2 staining at day 14 and 28 are shown for the proliferation groups in Figure 6. The staining results for the osteogenic group can be found in Figure S7, Supporting Information. Runx2 staining was positively correlated with mineral content and increased with culture time. Co-localization of Runx2 and DAPI staining confirmed that Runx2 staining was localized to the cell nuclei (Figure S8, Supporting Information).

OCN is a noncollagenous protein found in the ECM of bones and is involved in regulating mineralization.[40,41] OCN is a specific marker of osteoblasts and is therefore a useful marker for the late stages of osteogenesis.[42] The expression of OCN was muted in both groups at day 7. In the proliferation group, no positive staining could be found at locations 1−4 at day 14, although some positive staining was evident at location 5 (Figure 7, columns A−C). At day 28, in addition to location 5, OCN was observed at locations 3 and 4 (Figure 7, columns D−F). The staining result for the osteogenic group can be found in Figure S9, Supporting Information. In general, the level of OCN expression was positively correlated with mineral content along the length of the scaffold. Figure S10, Supporting Information, shows images of OCN expression at a higher magnification, demonstrating its localization to the ECM. These images also show the influence of nanofiber alignment on the arrangement of the cells, demonstrating that the cells were conformed to the anisotropic topography.

Discussion. ASCs demontrated either proliferative or differentiated phenotypes, depending on the local mineral content, culture condition, and culture time. Opposite trends were observed for these behaviors, indicating that the fate of the ASCs was controlled by chemical cues, compositional cues, and scaffold stiffness. Although cells were evenly distributed on scaffolds at the time of seeding, increased culture time resulted in more cells being present on the bare fibers than those mineralized. These differences in cell distribution became more prominent over time. This was consistent with the PCNA results, which showed that ASC proliferation was negatively correlated with the mineral content. Under the proliferation condition (i.e., in medium lacking osteogenic factors), the mineral content was sufficient to encourage ASCs toward osteogenic differentiation. At day 14, almost no cells exhibited positive PCNA staining at location 5, whereas ALP, Runx2, and OCN were highly expressed, indicating a shift from proliferation to differentiation that was correlated with the mineral content. Live/dead staining showed very few dead cells at any location on the scaffold, further supporting the interpretation that ASCs shifted from proliferation to differentiation after 14 days of culture due to the presence of mineral coating. These results are consistent with reports by others. For example, Triffitt and co-workers found that the proliferation of MSCs was reduced on mineral surfaces compared to plastics, while differentiation was enhanced by the presence of mineral.[43] Missirlis and co-workers reported lower proliferation and higher ALP activity for MSCs on hydroxyapatite (HA) than on culture plastics.[44] Nevertheless, contrasting results have also been reported by several groups. For example, Mooney and co-workers observed that MSCs grew faster on mineralized substrates, when compared to tissue culture plastics, whereas osteogenesis was inhibited by the presence of minerals.[45] This apparent contradiction may be explained by the differences in the type and morphology of minerals among the various studies. While HA promotes osteogenesis in most cases, tricalcium phosphate (TCP) can inhibit osteogenesis due to its low crystallinity, small crystal size, high surface roughness, and rapid dissolution rate relative to HA.[46−49] Consistent with the promotion of osteogenesis by HA, the mineral in the current study was primarily HA.[30]

Osteogenesis of ASCs changed gradually along the length of the mineralized scaffolds. ASCs showed no signs of osteogenesis on the unmineralized portion of the scaffold,

demonstrated an osteoprogenitor phenotype in the center of the scaffolds, and displayed an osteoblast phenotype on the fully mineralized portion of the scaffolds. These trends were reinforced with increasing culture time and by the use of osteogenic medium. Runx2 and OCN were chosen as representative early and late immunocytochemistry markers of osteogenesis, respectively.[34,41] Runx2 is a transcription factor necessary for early differentiation of MSCs into osteoprogenitors.[35] In contrast, OCN is primarily secreted by mature osteoblasts and osteocytes and is therefore a marker of mature bone cells.[42] Under the proliferation culture condition, a relatively large number of osteoprogenitor cells were evident at locations 4 and 5 by day 28. However, only a moderate number of mature osteoblasts was present at this time point. HA mineral is considered osteoconductive based on its capacity to promote osteogensis both *in vitro* and *in vivo*.[50−52] Huang and co-workers showed that both ALP activity and OCN expression of MSCs increased due to the introduction of HA into nanofibrous scaffolds.[53] Ramakrishna and co-workers electrosprayed HA onto electrospun nanofibers to enhance MSC differentiation.[54] The same group also precipitated HA onto electrospun nanofibers to induce the osteogenesis of ASCs.[55] Positive staining for both CD105 (an ASC-specific marker) and OCN showed that ASCs were undergoing osteogenesis due to the influence of HA. These and other results confirmed that polymer/mineral composite substrates can enhance the differentiation of MSCs by encouraging osteogenesis.[56]

The osteogenesis associated with mineral content may have been due to a compositional cue (i.e., mineral) or due to a mechanical cue (i.e., scaffold stiffness). The current study design did not allow for the separation of these two factors, as mineral content was directly related to scaffold stiffness.[20] Previous work has shown that the stiffness of the substrate itself can induce osteogenesis since integrin-mediated cell adhesion to matrix proteins is the first step that determines the fate of the stem cell and can therefore play an important role in osteogenesis.[57] Once integrins are bound to their ligands, they form specialized protein clusters called focal adhesions. These complexes ensure substrate adhesion and directed assembly of actin filaments. During osteogenesis, the morphology of cells changes from the fibroblast-like phenotype of a preosteoblast to the flattened and polygonal shape of the mature osteoblast.[58] The changes in the assembly and disassembly of the actin cytoskeleton are critical in supporting osteogenesis.[59,60] Since the stiffness of a substrate greatly affects the dynamics of actin assembly in individual cells, the enhanced stiffness of the scaffold due to incorporated minerals may also be a contributing factor to the enhanced osteogenesis.

Several limitations must be addressed before the scaffolds presented here can be used for *in vivo* studies. First, the current study only examined osteogenesis and did not explore tenogenesis. A complete stem cell therapy for tendon-to-bone repair should include both tenogenesis and osteogenesis in opposite gradients. Although it is feasible to deliver undifferentiated ASCs, with the hope that the local microenvironment will initiate appropriate differentiation, it is also worthwhile to investigate a method to induce tenogenesis on the scaffold presented here without compromising osteogenesis. Second, the study was not designed to mechanistically determine which factors drove the switch of ASCs from proliferation to osteogenesis. Additional studies need to be conducted to address these questions.

CONCLUSIONS

We have investigated the response of ASCs to nanofiber scaffolds, with spatial gradients in mineral content, under proliferative and osteogenic culture conditions. The ASCs attached to and/or proliferated at locations on the scaffolds with no or a low mineral content. High levels of mineral content remarkably enhanced the osteogensis of ASCs, independent of medium type. Local expressions of ALP, Runx2, and OCN were found to be positively correlated with the mineral content, resulting in a spatial gradient of cell phenotypes. This gradient in cell phenotypes largely mimics the cellular community of the native enthesis and is therefore a promising first step toward the regeneration of tendon-to-bone insertion. Further elucidation of ASC responses to the nanofiber scaffolds with spatial gradients in mineral content may provide a new approach to inducing targeted and localized cell differentiation for tissue engineering applications.

ASSOCIATED CONTENT

Supporting Information

Additional experimental data. This material is available free of charge via the Internet at http://pubs.acs.org/.

AUTHOR INFORMATION

Corresponding Authors

*E-mail: younan.xia@biomed.gatech.edu.
*E-mail: thomopouloss@wudosis.wustl.edu.

Present Address

[§]J.X.: Mary and Dick Holland Regenerative Medicine Program and Department of Pharmaceutical Sciences, University of Nebraska Medical Center, Omaha, Nebraska 68198, USA.

Notes

The authors declare no competing financial interest.

ACKNOWLEDGMENTS

This work was supported in part by a grant from the NIH (R01 AR060820) and startup funds from Georgia Institute of Technology (to Y.X.). Part of the work was performed at the Microscopy and Biophotonics Core in the Parker H. Petit Institute of Bioengineering and Bioscience. We thank Yu Shrike Zhang for his help with the preparation of this manuscript.

REFERENCES

(1) Wopenka, B.; Kent, A.; Pasteris, J. D.; Yoon, Y.; Thomopoulos, S. *Appl. Spectrosc.* **2008**, *62*, 1285−1294.
(2) Galatz, L. M.; Ball, C. M.; Teefey, S. A.; Middleton, W. D.; Yamaguchi, K. *J. Bone Jt. Surg., Am. Vol.* **2004**, *86*, 219−224.
(3) Thomopoulos, S.; Williams, G. R.; Soslowsky, L. J. *J. Biomech. Eng.* **2003**, *125*, 106−113.
(4) Thomopoulos, S.; Williams, G. R.; Gimbel, J. A.; Favata, M.; Solowsky, L. J. *J. Orthop. Res.* **2003**, *21*, 413−419.
(5) Smith, L.; Thomopoulos, S. *U.S. Musculoskeletal Dis.* **2011**, *6*, 11−15.
(6) Thomopoulos, S.; Genin, G. M.; Galatz, L. M. *J. Musculoskeletal Neuronal Interact.* **2012**, *10*, 35−45.
(7) Moffat, K. L.; Sun, W. H.; Pena, P. E.; Chahine, N. O.; Doty, S. B.; Ateshian, G. A.; Hung, C. T.; Lu, H. H. *Proc. Natl. Acad. Sci. U.S.A.* **2008**, *105*, 7947−7952.
(8) Smith, L.; Xia, Y.; Galatz, L. M.; Genin, G. M.; Thomopoulos, S. *Connect. Tissue Res.* **2012**, *53*, 95−105.
(9) Doschak, M. R.; Zernicke, R. F. *J. Musculoskeletal Neuronal Interact.* **2005**, *5*, 35−40.
(10) Spalazzi, J. P.; Doty, S. B.; Moffat, K. L.; Levine, W. N.; Lu, H. H. *Tissue Eng.* **2006**, *24*, 2001−2010.

(11) Liu, W.; Yeh, Y.-C.; Lipner, J.; Xie, J.; Sung, H.-W.; Thomopoulos, S.; Xia, Y. *Langmuir* **2011**, *27*, 9088−9093.
(12) Xie, J.; Li, X.; Lipner, J.; Manning, C. N.; Schwartz, A. G.; Thomopoulos, S.; Xia, Y. *Nanoscale* **2010**, *6*, 923−926.
(13) Liu, W.; Zhang, Y. S.; Thomopoulos, S.; Xia, Y. *Angew. Chem., Int. Ed.* **2012**, *52*, 420−432.
(14) Lu, H. H.; Subramony, S. D.; Boushell, M. K.; Zhang, X. *Ann. Biomed. Eng.* **2010**, *38*, 2142−2154.
(15) Xie, J.; Li, X.; Xia, Y. *Macromol. Rapid Commun.* **2008**, *29*, 1775−1792.
(16) Xie, J.; Blough, E. R.; Wang, C. H. *Acta Biomater.* **2012**, *8*, 811−819.
(17) Liu, W.; Thomopoulos, S.; Xia, Y. *Adv. Healthcare Mater.* **2012**, *1*, 10−25.
(18) Li, D.; Xia, Y. *Adv. Mater.* **2004**, *16*, 1151−1170.
(19) Pham, Q. P.; Sharma, U.; Mikos, A. G. *Tissue Eng.* **2006**, *12*, 1197−1211.
(20) Li, X.; Xie, J.; Lipner, J.; Yuan, X.; Thomopoulos, S.; Xia, Y. *Nano Lett.* **2009**, *9*, 2763−2768.
(21) Gimble, J. M. *Expert Opin. Biol. Ther.* **2003**, *3*, 705−713.
(22) Gimble, J. M.; Katz, A. J.; Bunnell, B. A. *Circ. Res.* **2007**, *100*, 1249−1260.
(23) Niemeyer, P.; Kornacker, M.; Mehlhorn, A.; Seckinger, A.; Vohrer, J.; Schmal, H.; Kasten, P.; Eckstein, V.; Sudkamp, N. P.; Krause, U. *Tissue Eng.* **2007**, *13*, 111−121.
(24) Faqng, B.; Song, Y.; Liao, L.; Zhang, Y.; Zhao, R. C. *Transplant. Proc.* **2007**, *39*, 3358−3362.
(25) Yanez, R.; Lamana, M. L.; Garcia-Castro, J.; Colmenero, I.; Ramirez, M.; Bueren, J. A. *Stem Cells* **2006**, *24*, 2582−2591.
(26) Tas, A. C.; Bhaduri, S. B. *J. Mater. Res.* **2004**, *19*, 2742−2749.
(27) Guilak, F.; Lott, K. E.; Awad, H. A.; Cao, Q.; Hicok, K. C.; Fermor, B.; Gimble, J. M. *J. Cell Physiol.* **2006**, *206*, 229−237.
(28) Shen, H.; Gelberman, R. H.; Silva, M. J.; Sakiyama-Elbert, S. E.; Thomopoulos, S. *PLoS One* **2013**, *8*, No. e77613.
(29) Pham, Q. P.; Sharma, U.; Mikos, A. G. *Biomacromoles* **2006**, *7*, 2796−2805.
(30) Li, X.; Xie, J.; Yuan, X.; Xia, Y. *Langmuir* **2008**, *24*, 14145−14150.
(31) Yang, F.; Wolke, J. G. C.; Jansen, J. A. *Chem. Eng. J.* **2008**, *137*, 154−161.
(32) Robison, R. *Biochem. J.* **1923**, *17*, 286−293.
(33) Marom, R.; Shur, I.; Solomon, R.; Benayahu, D. *J. Cell Physiol.* **2005**, *202*, 41−48.
(34) Golub, E. E.; Boesze-Battaglia, K. *Curr. Opin. Orthopaed.* **2007**, *18*, 444−448.
(35) Pratap, J.; Galindo, M.; Zaidi, S. K.; Vradii, D.; Bhat, B. M.; Robinson, J. A.; Choi, J.-Y.; Komori, T.; Stein, J. L.; Lian, J. B.; Stein, G. S.; Wijnen, A. J. *Cancer Res.* **2003**, *63*, 5357−5362.
(36) Ducy, P.; Zhang, R.; Geoffroy, V.; Ridall, A. L.; Karsenty, G. *Cell* **1997**, *89*, 747−754.
(37) Komori, T. *J. Cell Biochem.* **2005**, *95*, 445−453.
(38) Komori, T. *Adv. Exp. Med. Biol.* **2010**, *658*, 43−49.
(39) Otto, F.; Thornell, A. P.; Crompton, T.; Denzel, A.; Gilmour, K. C.; Rosewell, I. R.; Stamp, G. W. H.; Beddington, R. S. P.; Mundlos, S.; Olsen, B. R.; Selby, P. B.; Owen, M. J. *Cell* **1997**, *89*, 765−771.
(40) Hauschka, P. V.; Lian, J. B.; Cole, D. E.; Gundberg, C. M. *Physiol. Rev.* **1989**, *69*, 990−1047.
(41) Harada, S.; Rodan, G. A. *Nature* **2003**, *423*, 349−355.
(42) Lee, N. K.; Sowa, H.; Hinoi, E.; Ferron, M.; Ahn, J. D.; Confavreux, C.; Dacquin, R.; Mee, P. J.; McKee, M. D.; Jung, D. Y.; Zhang, Z.; Kim, J. K.; Mauvais-Jarvis, F.; Ducy, P. *Cell* **2007**, *130*, 456−469.
(43) Oreffo, R. O. C.; Driessens, F. C. M.; Planell, J. A.; Triffitt, J. T. *Biomaterials* **1998**, *19*, 1845−1854.
(44) Deligianni, D. D.; Katsala, N. D.; Koutsoukos, P. G.; Missirlis, Y. F. *Biomaterials* **2001**, *2*, 87−96.
(45) Murphy, W. L.; Hsiong, S.; Richardson, T. P.; Simmons, C. A.; Mooney, D. J. *Biomaterial* **2005**, *26*, 303−310.
(46) Chou, L.; Marek, B.; Wagner, W. R. *Biomaterials* **1999**, *20*, 977−985.
(47) Chang, Y. L.; Stanford, C. M.; Keller, J. C. *J. Biomed. Mater. Res.* **2000**, *52*, 270−278.
(48) Meleti, Z.; Shapiro, I. M.; Adams, C. S. *Bone* **2000**, *27*, 359−366.
(49) Ong, J. L.; Hoppe, C. A.; Cardenas, H. L.; Cavin, R.; Carnes, D. L.; Sogal, A.; Raikar, G. N. *J. Biomed. Mater. Res.* **1998**, *39*, 176−183.
(50) Kaito, T.; Myoui, A.; Takaoka, K.; Saito, N.; Nishikawa, M.; Tamai, N.; Ohgushi, H.; Yoshikawa, H. *Biomaterials* **2005**, *26*, 73−79.
(51) Zhang, P.; Hong, Z.; Yu, T.; Chen, X.; Jing, X. *Biomaterials* **2009**, *30*, 58−70.
(52) Kim, S. S.; Park, M. S.; Jeon, O.; Choi, C. Y.; Kim, B. S. *Biomaterials* **2006**, *27*, 1399−1409.
(53) Lu, L. X.; Zhang, X. F.; Wang, Y. Y.; Ortiz, L.; Mao, X.; Jiang, Z. L.; Xiao, Z. D.; Huang, N. P. *ACS Appl. Mater. Interfaces* **2013**, *5*, 319−330.
(54) Venugopal, J.; Rajeswari, R.; Shayanti, M.; Low, S.; Bongso, A.; Dev, V. R.; Deepika, G.; Choon, A. T.; Ramakrishna, S. *J. Biomater. Sci., Polym. Ed.* **2012**, *24*, 170−184.
(55) Ravichandran, R.; Venugopal, J. R.; Sundarrajan, S.; Mukherjee, S.; Ramakrishna, S. *Biomaterials* **2012**, *33*, 846−855.
(56) Mygind, T.; Stiehler, M.; Baatrup, A.; Li, H.; Zou, X.; Flyvbjerg, A.; Kassem, M.; Bunger, C. *Biomaterials* **2007**, *28*, 1036−1047.
(57) Scadden, D. T. *Nature* **2006**, *441*, 1075−1079.
(58) Rodriguez, J. P.; Gonzalez, M.; Rios, S.; Cambiazo, V. *J. Cell Biochem.* **2004**, *93*, 721−731.
(59) Yourek, G.; Hussain, M. A.; Mao, J. J. *ASAIO J.* **2007**, *53*, 219−228.
(60) MaBeath, R.; Pirone, D. M.; Nelson, C. M.; Bhadriraju, K.; Chen, C. S. *Dev. Cell* **2004**, *6*, 483−495.